Electronic Supplementary Material (ESI) for Inorganic Chemistry Frontiers.

Catalytic reactions in a Co_{12} cuboctahedral cage arising from guest encapsulation and cage-based redox activation

Xuejian Zhang, Burin Sudittapong and Michael D. Ward*

Supporting information

1. Cage synthesis and characterisation

Ligands **L^{mes}** and **L^{ph}** were synthesised and purified according to previously published methods (main text, ref. 11a). Catalysis experiments were monitored by UV/Vis spectral absorption changes using previously-reported methodology and instrumentation (main text, refs. 6e, 6g).

Preparation of $[Co_{12}(L^{mes})_4(L^{ph})_{12}](BF_4)_{24}$ (Co_{12}). *This synthesis follows that previous reported (main text, ref.11a).* To a mixture of ligands L^{mes} (50.0 mg, 0.085 mmol) and L^{ph} (100 mg, 0.262 mmol) dissolved in $MeNO_2$ (20 cm^3) was added a methanolic solution (2 cm^3) of $Co(BF_4)_2$ (93 mg, 0.275 mmol), leading to an immediate colour change to a bright yellow solution. The solution was stirred overnight at room temperature before removing solvents under reduced pressure to afford a yellow solid. The crude product was further purified by dissolved in a minimum amount of acetonitrile (*ca.* 1 cm^3), and to this solution was added ethyl acetate was added to give a yellow crystalline powder which was dried in *vacuo* (yield: 200 mg, 80%).

HR-ESI-MS data (Fig. S1, S2) and ^{1}H NMR data (Fig. S3, S4) for **Co_{12}** are in the figures on the next pages.

The analogous Zn(II) complex **$[Zn_{12}(L^{mes})_4(L^{ph})_{12}](BF_4)_{24}$ (Zn_{12})** used for control experiments was prepared identically and with a similar yield, see Fig. S5 – S6 for its ES mass spectrum and Fig. S7, S8 for ^{1}H NMR spectral data.

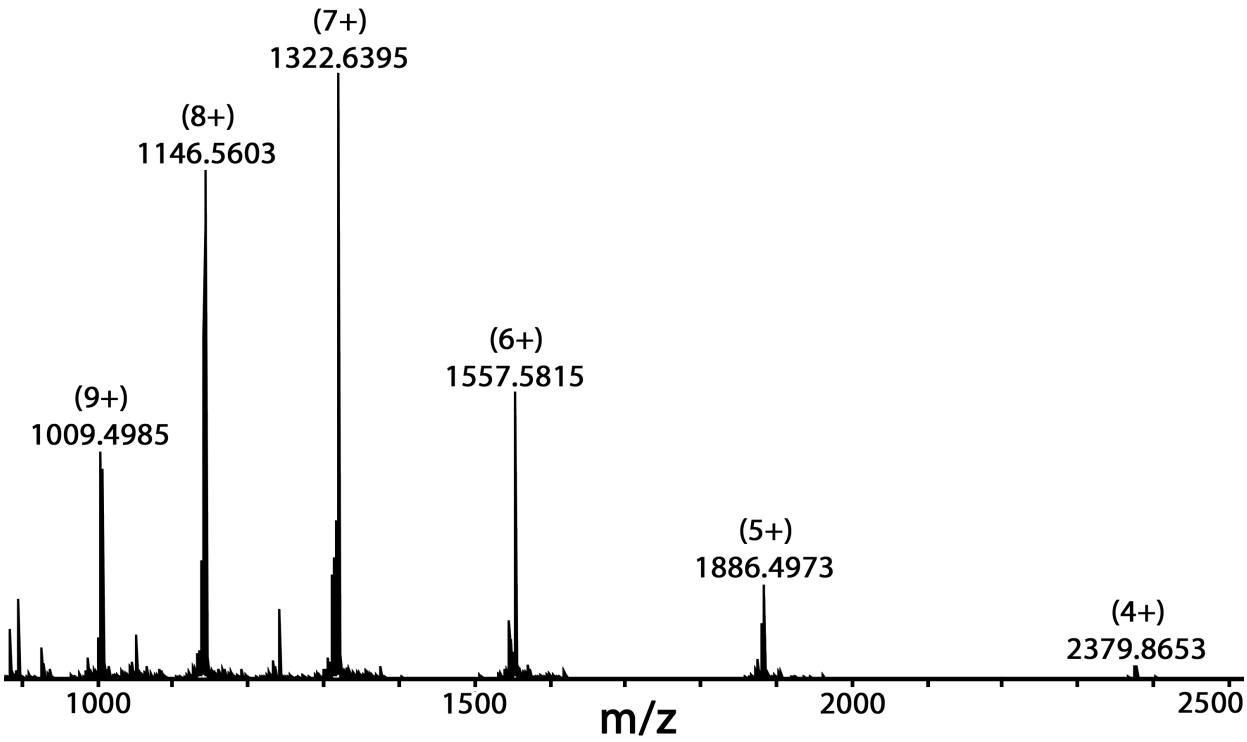

Fig. S1: ES mass spectrum of $[Co_{12}(L^{mes})_4(L^{ph})_{12}](BF_4)_{24}$ in (top panel) water / MeCN (9:1) showing the sequence $\{\mathbf{Co_{12}} - n(BF_4^-)\}^{n+}$ (n = 4 – 9) associated with sequential loss of anions.

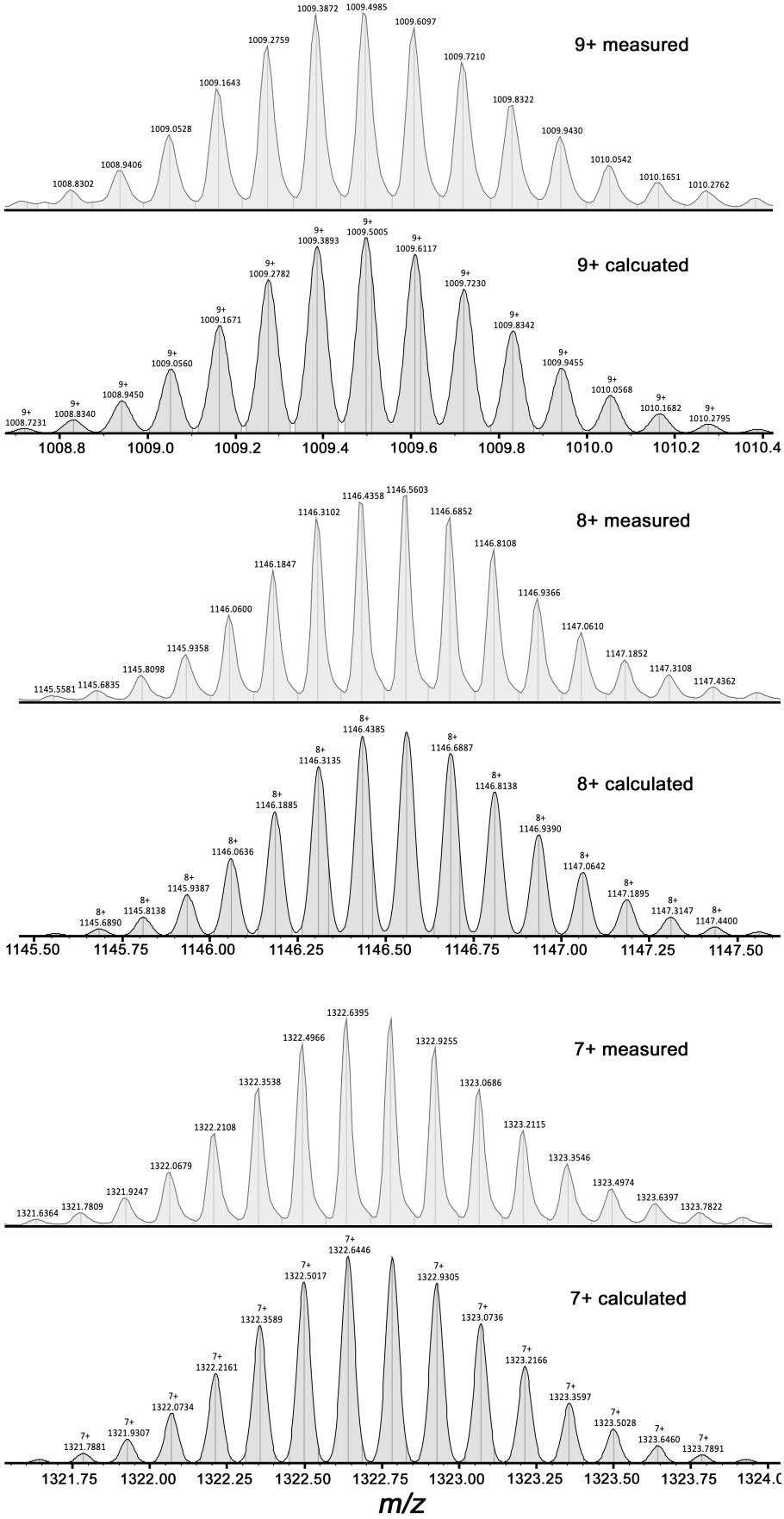

Fig. S2: ES mass spectrum of $[Co_{12}(L^{mes})_4(L^{ph})_{12}](BF_4)_{24}$ showing expansions of the signals for the signals $\{\mathbf{Co_{12}} - n(BF_4^-)\}^{n+}$ (n = 7, 8, 9) together with calculated spectra.

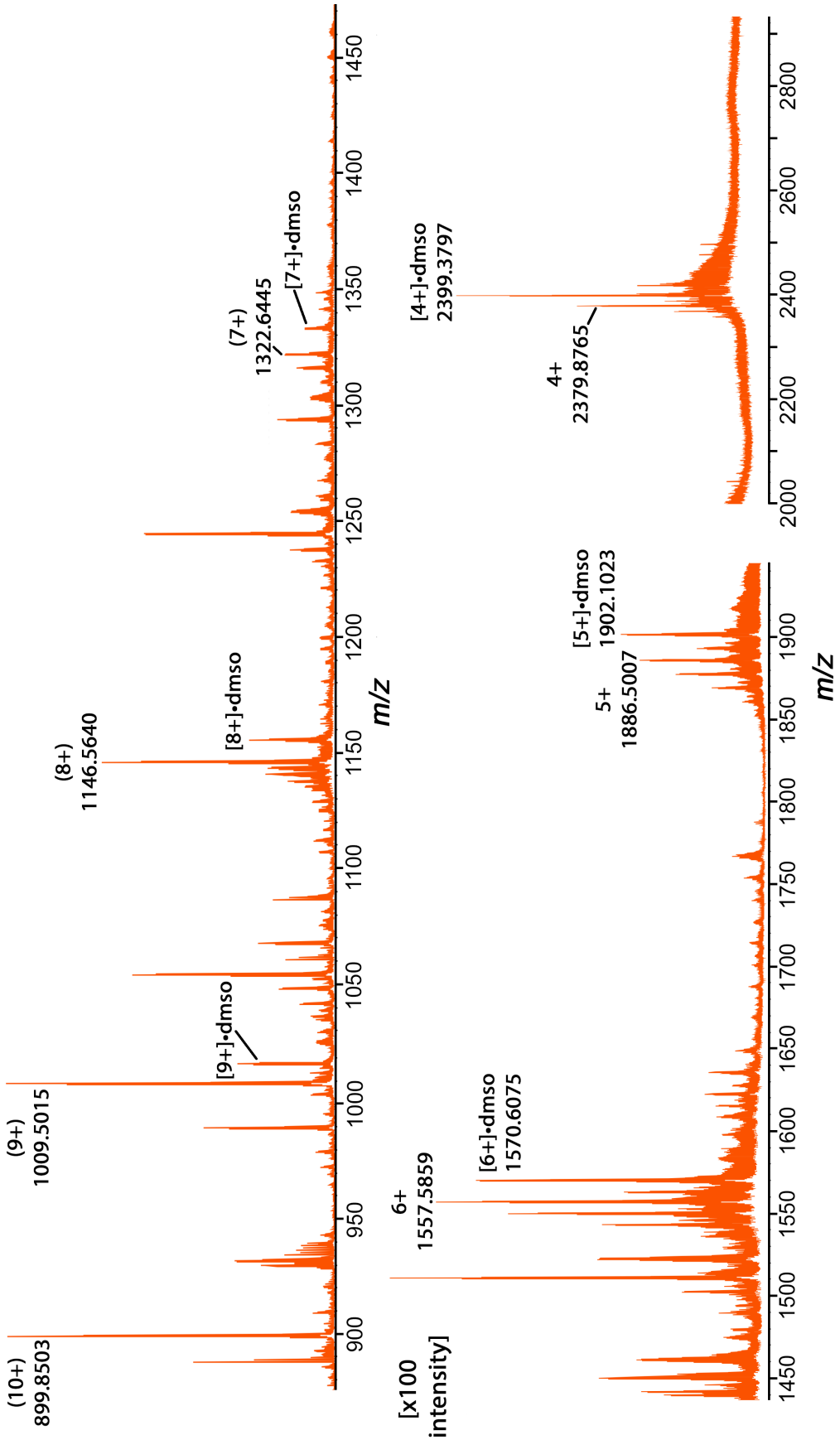

Fig. S3: Additional ES mass spectrum of $[Co_{12}(L^{mes})_4(L^{ph})_{12}](BF_4)_{24}$ in water / dmso (99:1) showing the sequence $\{\mathbf{Co_{12}} - n(BF_4^-)\}^{n+}$ (n = 4 – 10) associated with sequential loss of anions. In this case more fragmentation can be seen than in water / MeCN (9:1), and some dmso adducts are visible, but signals corresponding to the intact complex are clear.

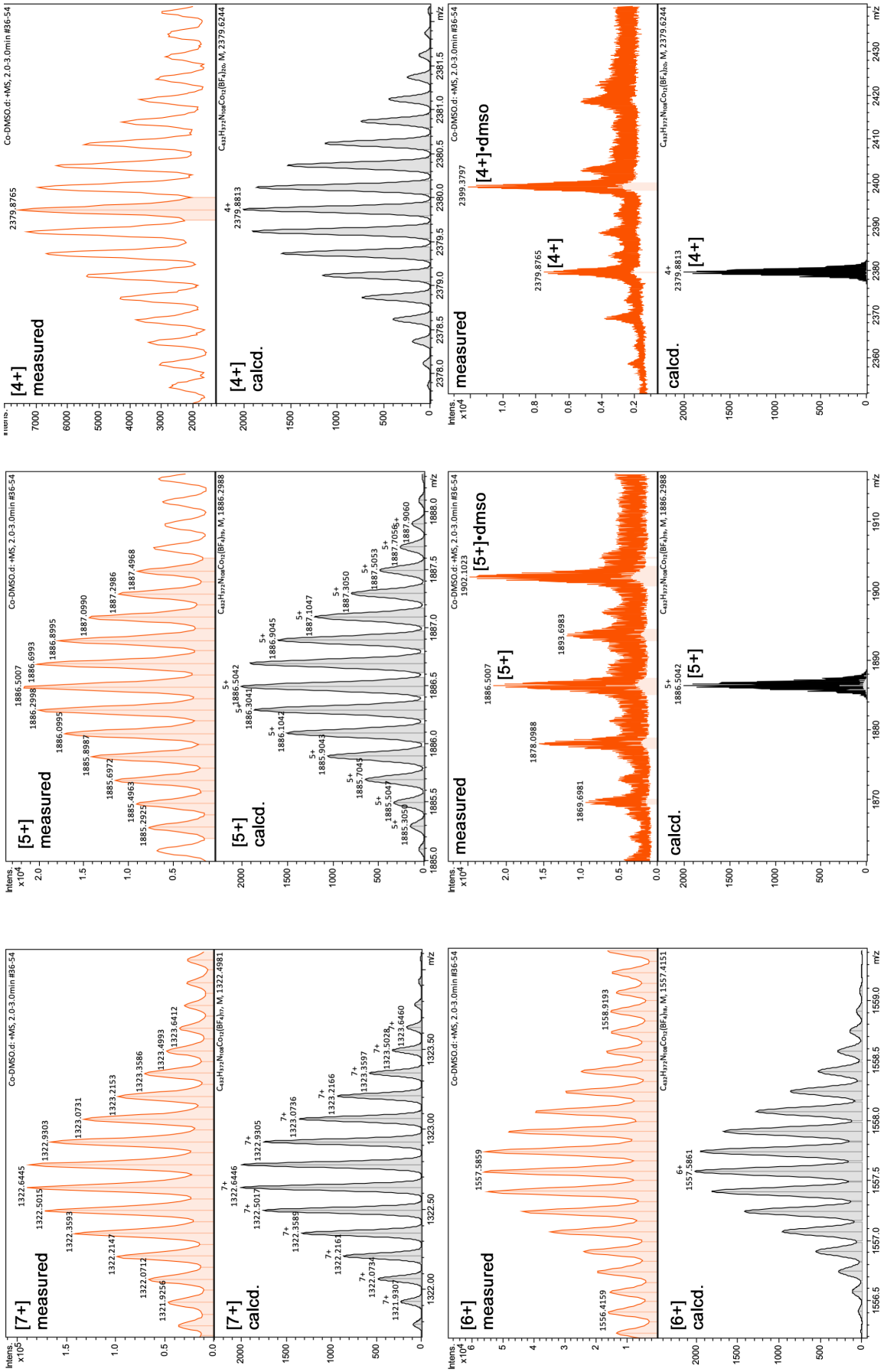

Fig. S4. Expansions of selected signals from the spectrum in Fig. S3 including calculated isotope patterns.

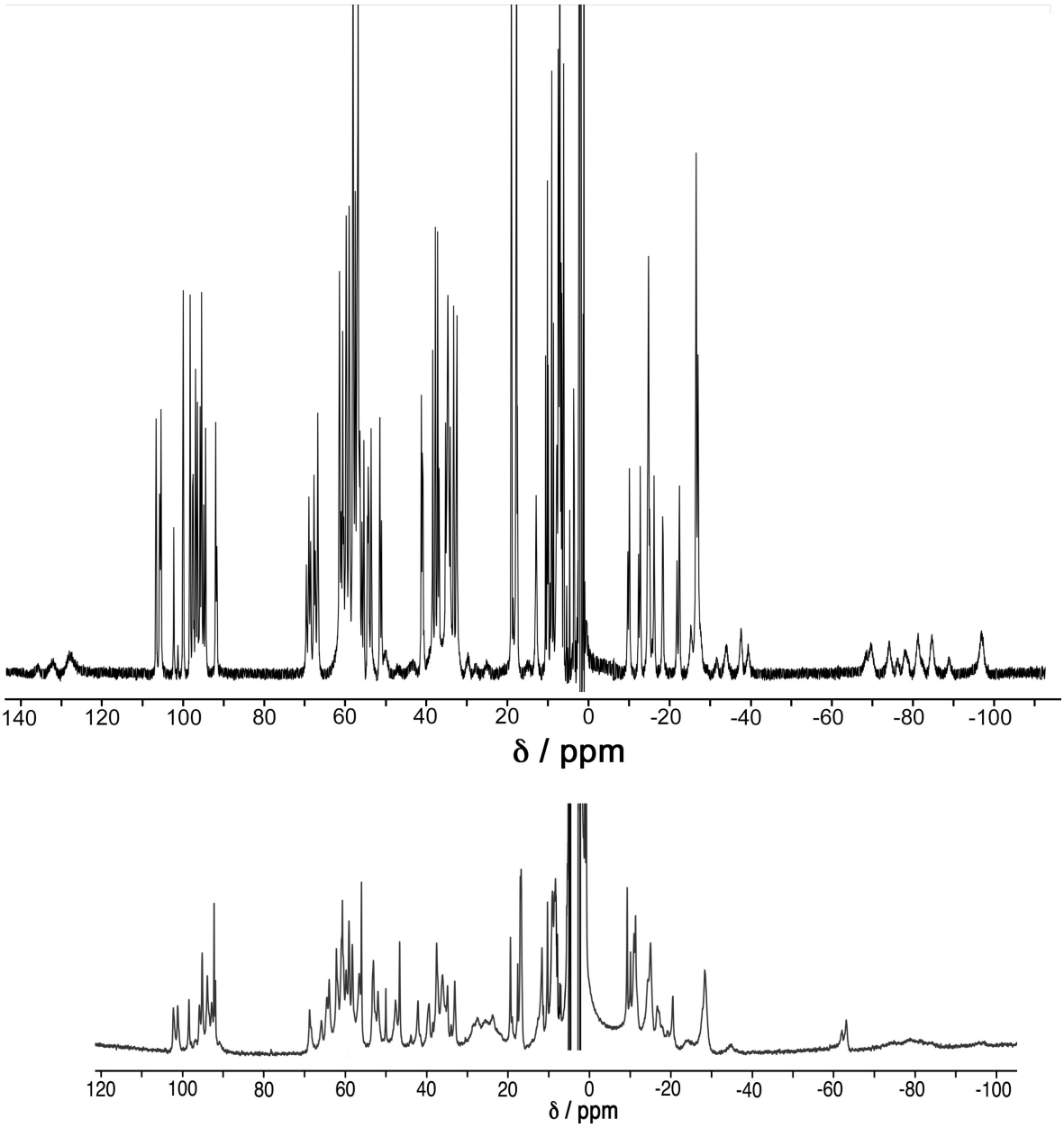

Fig. S5: ^{1}H NMR spectra (300 MHz, RT) of $[Co_{12}(L^{mes})_4(L^{ph})_{12}](BF_4)_{24}$ (mixture of three diastereoisomers, see main text, ref. 11b). The spectrum in 1% dmso / 99% D_2O – conditions used for many of the catalysis experiments – is considerably broader because of the higher viscosity of the mostly aqueous solvent, see especially the signals in the region -60 to -100 ppm, but the correspondence between the two is clear. Note that the paramagnetism prevents a DOSY spectrum form being recorded, but the integrity of **Co_{12}** in this solvent is also clear from the mass spectra. An expansion of parts of the MeCN spectrum are in the next figure.

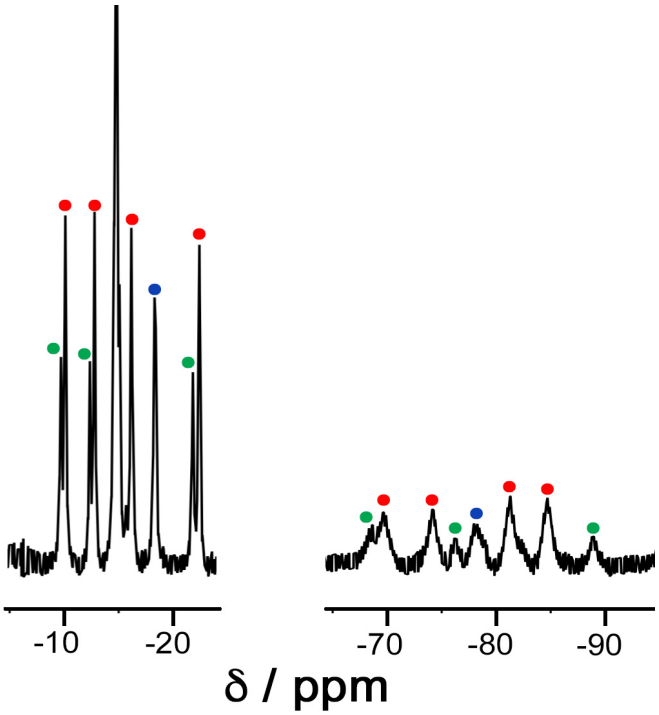

Fig. S6: Some expansions of the spectrum of $[Co_{12}(L^{mes})_4(L^{ph})_{12}](BF_4)_{24}$ in MeCN (Fig. S3, top panel) showing regions where the set of 8 signals (with three subsets of 4, 3 and 1, indicated by coloured dots) for each proton type in the mixture of three diastereoisomers can be discerned. These are the C_3 (red dots, four environments), S_4 (green dots, three environments) and *T* (blue dot, one environment) diastereoisomers – see main text (ref. 11b) for a detailed explanation.

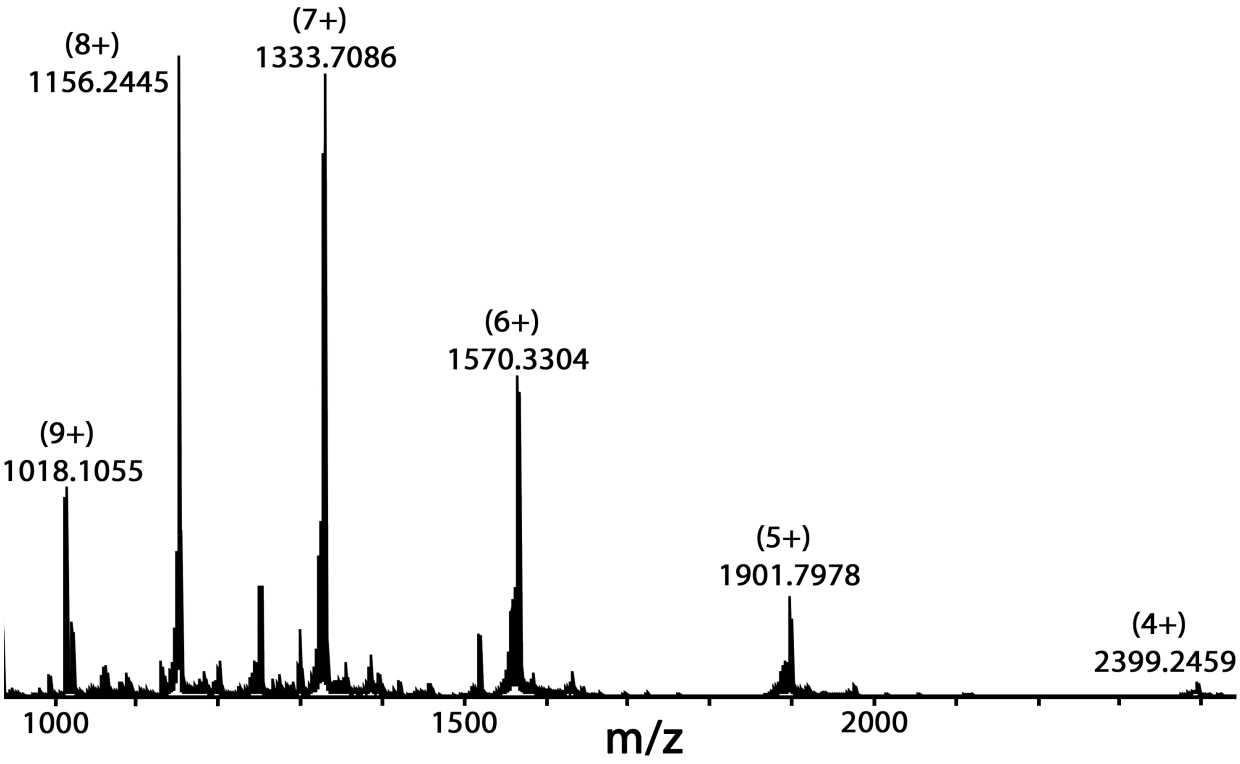

Fig. S7: ES mass spectrum of $[Zn_{12}(L^{mes})_4(L^{ph})_{12}](BF_4)_{24}$ in water / MeCN (9:1) showing the sequence $\{\mathbf{Zn_{12}} - n(BF_4^-)\}^{n+}$ (n = 4 – 9) associated with sequential loss of anions.

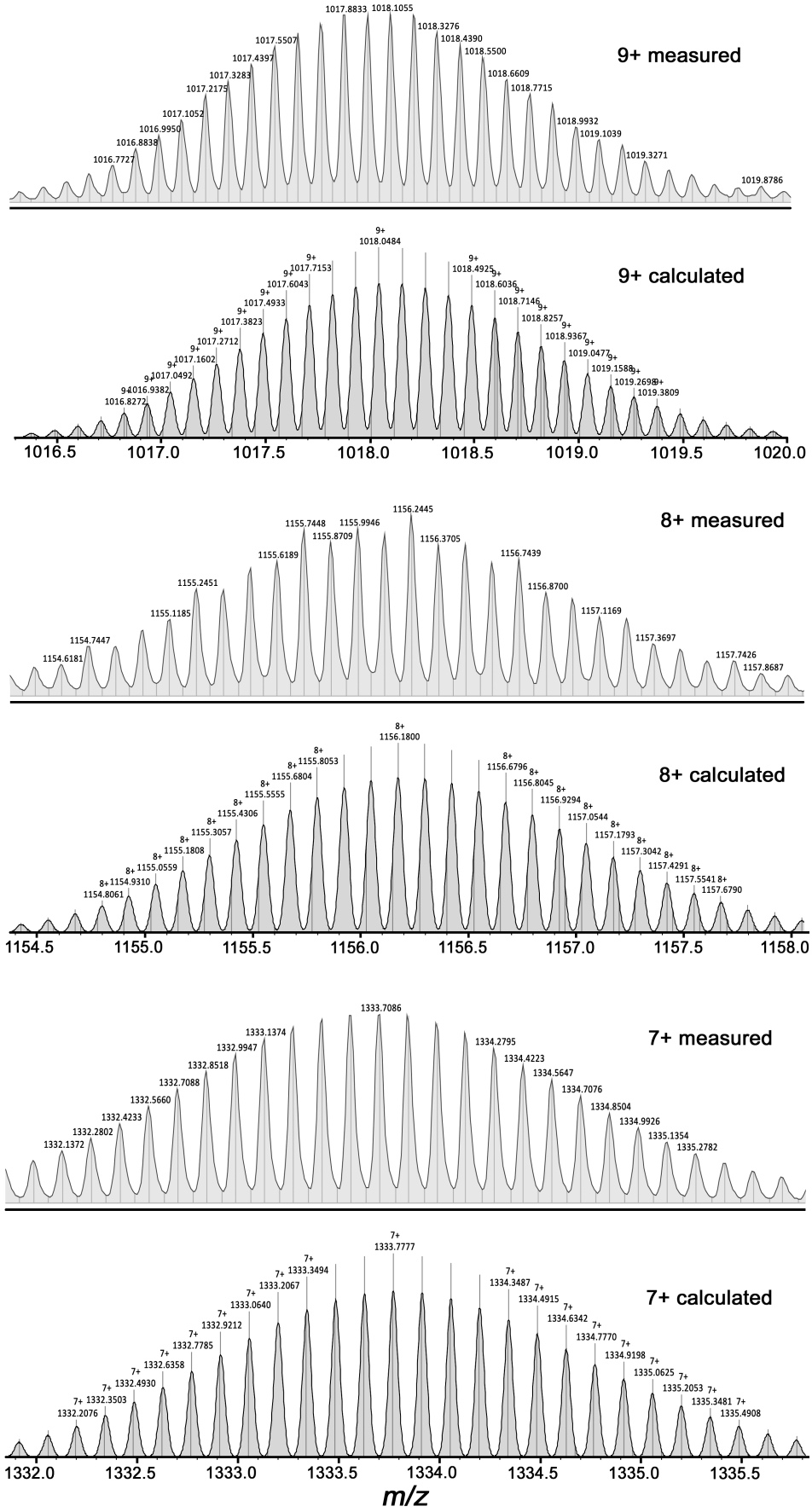

Fig. S8: ES mass spectrum of $[Zn_{12}(L^{mes})_4(L^{ph})_{12}](BF_4)_{24}$ in water / MeCN (9:1) showing expansions of the signals for $\{\mathbf{Zn_{12}} - n(BF_4^-)\}^{n+}$ (n = 7, 8, 9) together with calculated spectra.

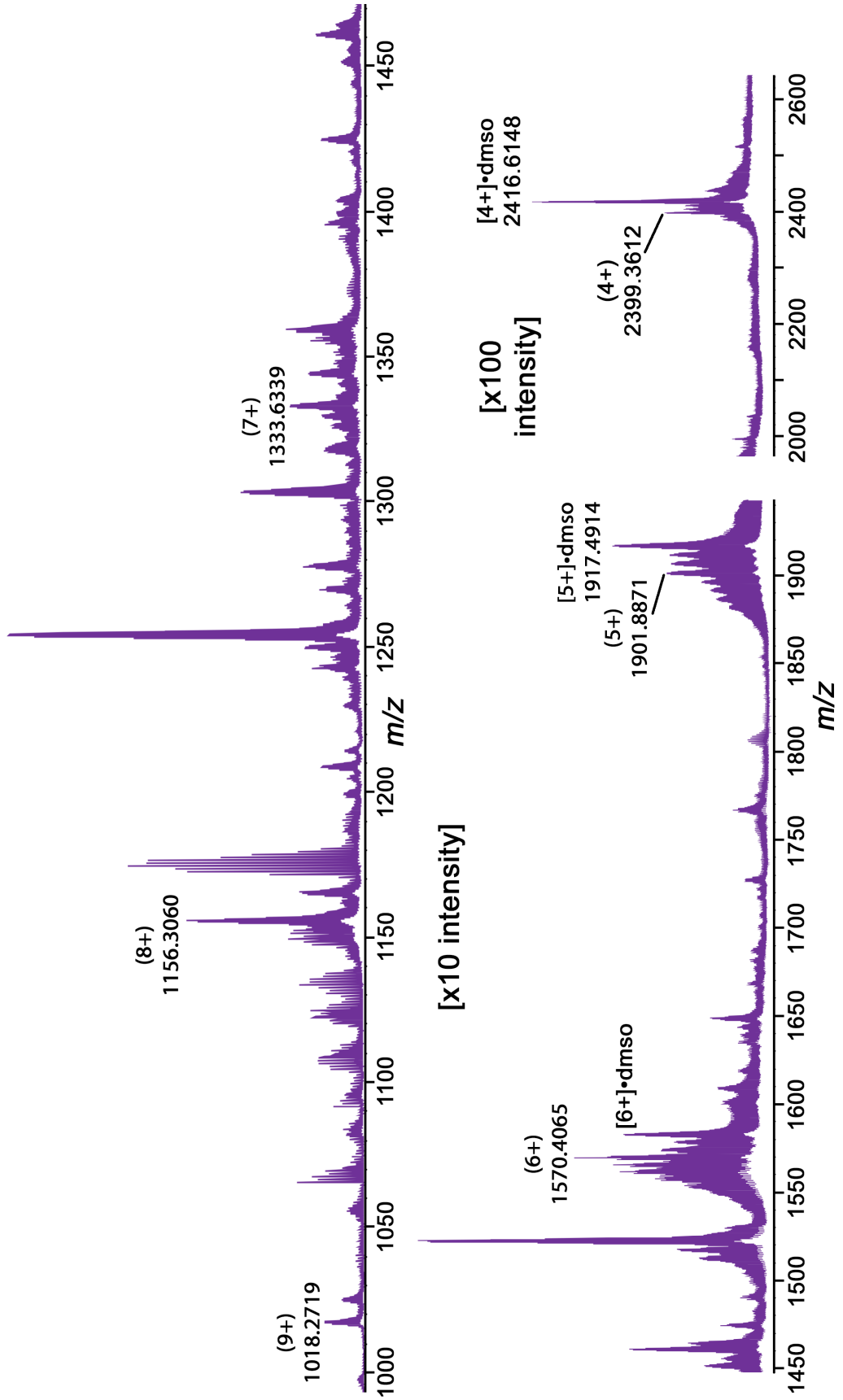

Fig. S9: Additional ES mass spectrum of $[Zn_{12}(L^{mes})_4(L^{ph})_{12}](BF_4)_{24}$ in water / dmso (99:1) showing the sequence $\{\mathbf{Zn_{12}} - n(BF_4^-)\}^{n+}$ (n = 4 – 9) associated with sequential loss of anions. As with the **Co_{12}** analogue (Fig. S3) more fragmentation can be seen than in water / MeCN (9:1), and some dmso adducts are visible, but signals corresponding to the intact complex are clear.

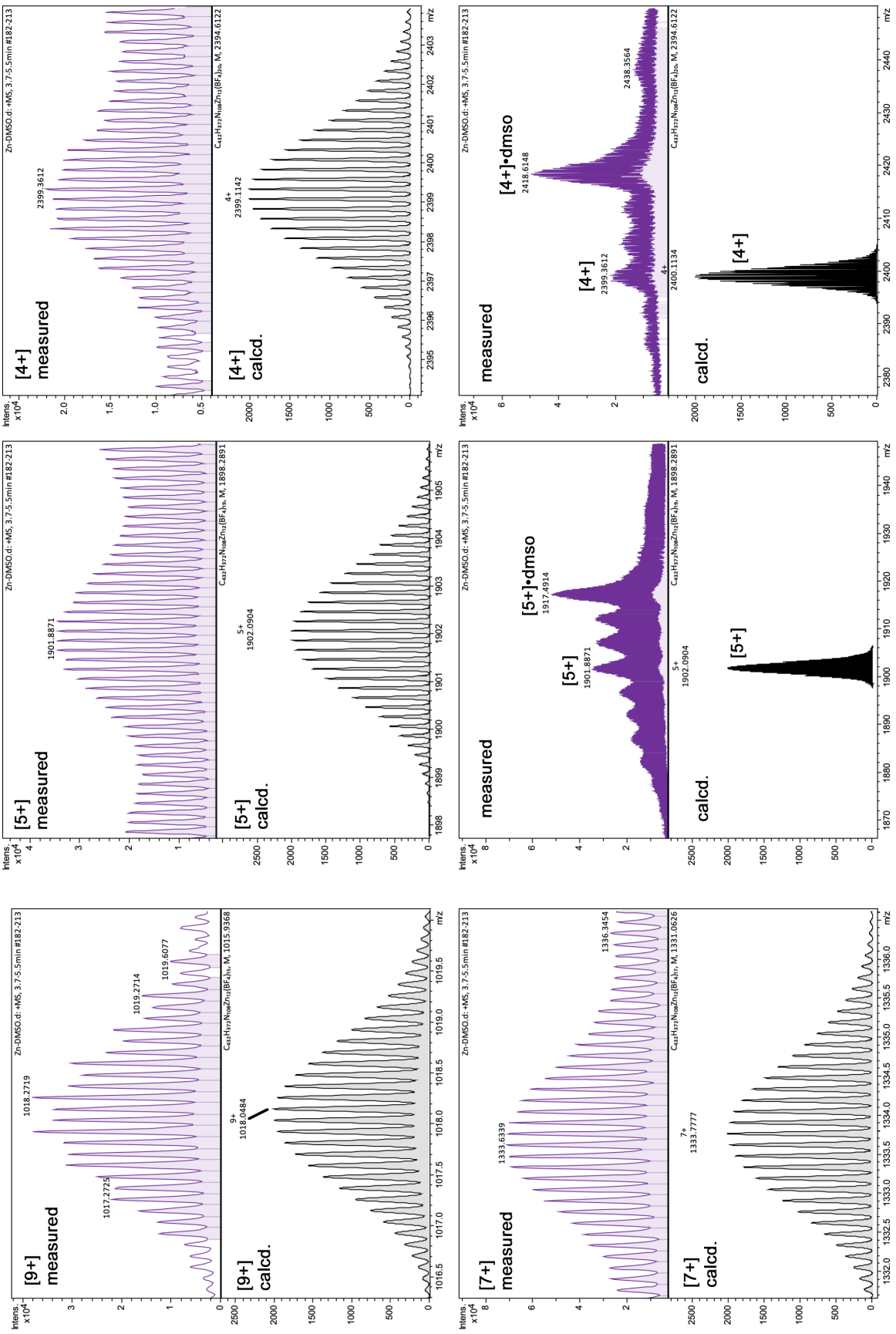

Fig. S10. Expansions of selected signals from the spectrum in Fig. S9 including calculated isotope patterns.

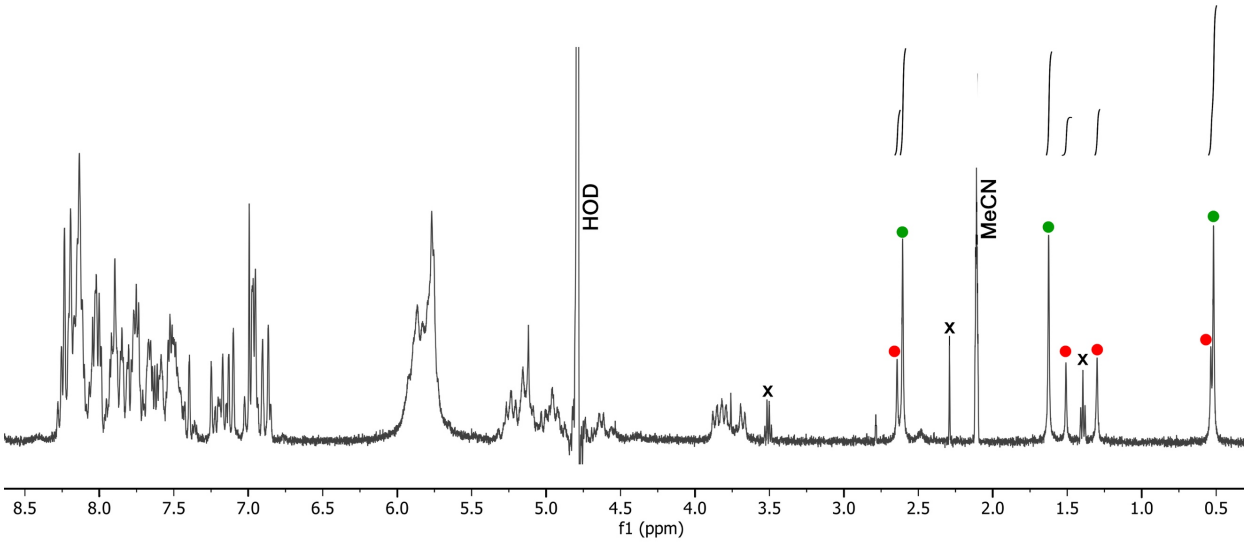

Fig S11. 500 MHz ^{1}H NMR spectrum of $[Zn_{12}(L^{mes})_4(L^{ph})_{12}](BF_4)_{24}$ in MeCN / D_2O (1:9) – the solvent system was chosen to confirm cage stability in an aqueous environment, with 10% MeCN needed for solubility purposes. The methyl signals from the L^{mes} ligand clearly show the presence of the C_3 (red dots, four equal-intensity environments), S_4 (green dots, three equal-intensity environments) diastereoisomers – see main text (ref. 11b) for a detailed explanation. The additional single signal expected from the *T* isomer is not observable, indicating either that this diastereoisomer is not significant in the solution equilibrium for this complex, or that the signal is hidden by the MeCN peak. Signals marked **x** are from traces of residual solvents (diethyl ether, 1.4 and 3.5 ppm; acetone, 2.3 ppm) and do not feature in the DOSY spectrum (next figure).

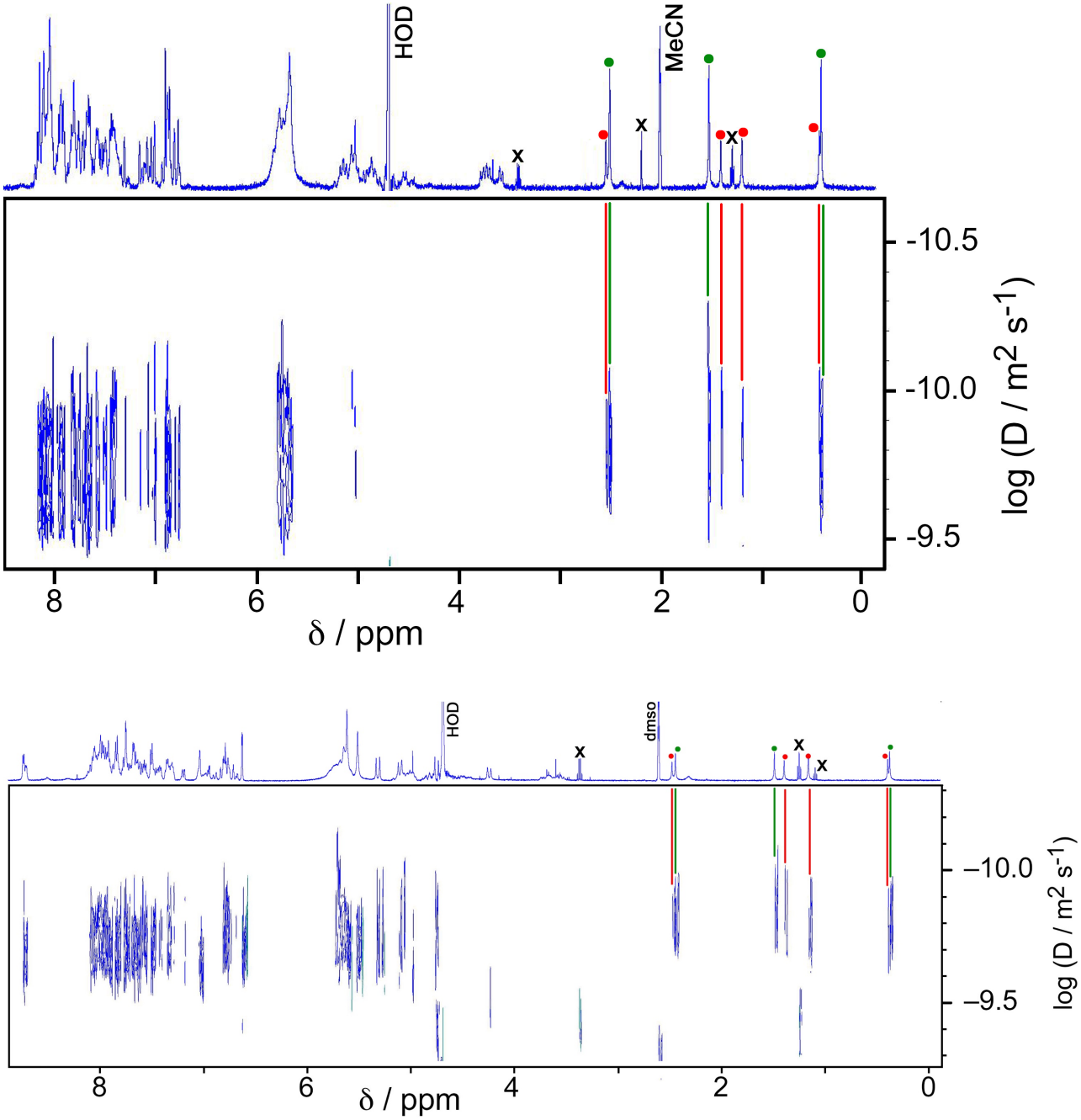

Fig. S12. ^{1}H DOSY NMR spectra of $[Zn_{12}(L^{mes})_4(L^{ph})_{12}](BF_4)_{24}$ in (top panel) MeCN / D_2O (1:9) and (bottom panel) dmso / D_2O (3:97) confirming the presence of a single species with a log (D /m^2 s^{-1}) value of -9.8; see main text for analysis. Notably the methyl groups indicated by the red and green dots (from different diastereoisomers) are present in the DOSY spectra, see red and green vertical lines indicating the correspondences. Residual solvent traces (signals labelled **x**) clearly have no correspondences in the main part of the DOSY spectrum corresponding to the intact cage.

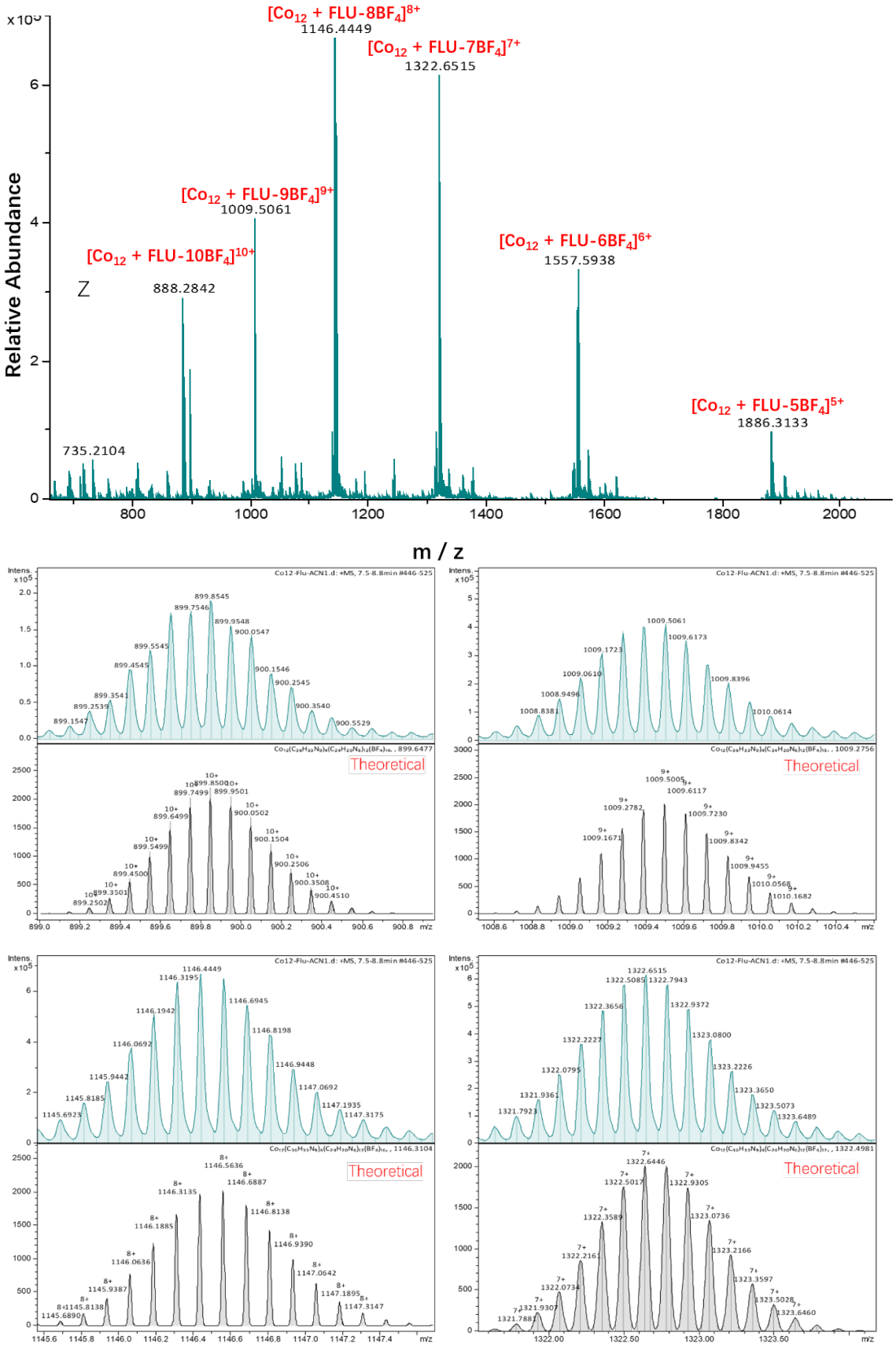

Fig. S13: ES mass spectrum of $[Co_{12}(L^{mes})_4(L^{ph})_{12}](BF_4)_{24}$ + fluorescein in MeCN showing formation of the 1:1 **Co_{12}•FLU** complex, with expansions (plus calculated simulations) for the 10+, 9+, 8+ and 7+ signals arising from loss of BF_4^- ions.

2. Preparation of aqueous solution of Co_{12} using a surfactant (Tween 20)

A sample of **Co_{12}** (15 mg, 1.51 µmol) was weighed and placed in a 20 ml sample vial. 0.22 g Tween20 (*ca.* 0.2 cm^3) was carefully weighed and added into the vial by a glass pipette. The resulting viscous mixture was stirred vigorously and thoroughly overnight. 2 cm^3 deionized water was added to the vial and the suspension was sonicated for 5 minutes. The mixture was stirred for another 30 minutes and a yellow transparent solution was obtained (see picture below) The resulting sample was further purified by filtering through a 2 µm syringe filter to remove any insoluble dust and impurities. The micelle size distribution was determined by dynamic light scattering (see picture below).

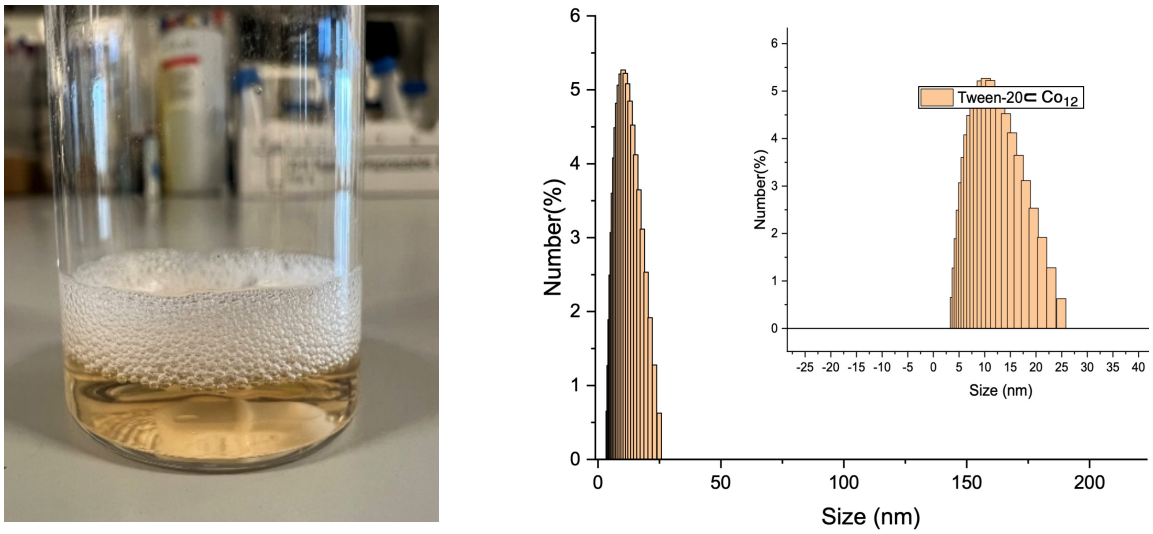

Fig. S14. Left: aqueous solution of **TW20⊂Co_{12}** prepared according to the procedure above. Right: DLS analysis of micelle size distribution showing a peak centred around the 12 nm region.

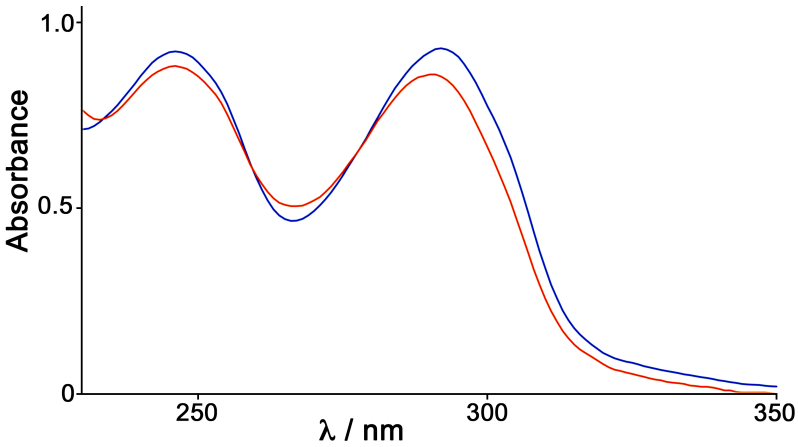

Fig. S15: Comparison of UV/Vis absorption spectra of **Co_{12}** in MeCN (orange curve) and in water/dmso (99:1) (blue curve) with a 1 cm path length (concentration 0.0278 M).

3. Catalysis of phosphate esters

Table S1. Summary of rate constants for catalysed hydrolysis of Me-paraoxon and Et-paraoxon by **TW20⊂Co$_{12}$** (data shown in Fig. 3 of the main text)

Substrate	Catalyst	k_{cat}(s^{-1})*	k_2 ($M^{-1}s^{-1}$)
Me-Paraoxon	1 mol% TW20 ⊂ **Co$_{12}$**	2.0 x 10^{-6}	0.50
	4 mol% TW20 ⊂ **Co$_{12}$**	9.2 x 10^{-6}	0.48
	8 mol% TW20 ⊂ **Co$_{12}$**	1.9 x 10^{-5}	0.48
	1 mol% **Co$_{12}$** (1% DMSO)	0.9 x 10^{-6}	0.23
	4 mol% **Co$_{12}$** (1% DMSO)	4.1 x 10^{-6}	0.21
	8 mol% **Co$_{12}$** (1% DMSO)	5.6 x 10^{-6}	0.14
Et-paraoxon	1 mol% TW20 ⊂ **Co$_{12}$**	1.0 x 10^{-6}	0.44
	4 mol% TW20 ⊂ **Co$_{12}$**	4.6 x 10^{-6}	0.46
	8 mol% TW20 ⊂ **Co$_{12}$**	8.1 x 10^{-6}	0.46
	1 mol% **Co$_{12}$** (1% DMSO)	0.6 x 10^{-6}	0.26
	4 mol% **Co$_{12}$** (1% DMSO)	1.9 x 10^{-6}	0.19
	8 mol% **Co$_{12}$** (1% DMSO)	3.5 x 10^{-6}	0.20
Diacetyl Fluorescein	2 mol% **Co$_{12}$** (1% DMSO)	1.0 x 10^{-6}	0.20
	20 mol% **Co$_{12}$** (1% DMSO)	1.2 x 10^{-5}	0.24

* Corrected by subtraction of the rate for the background (uncatalysed) hydrolysis

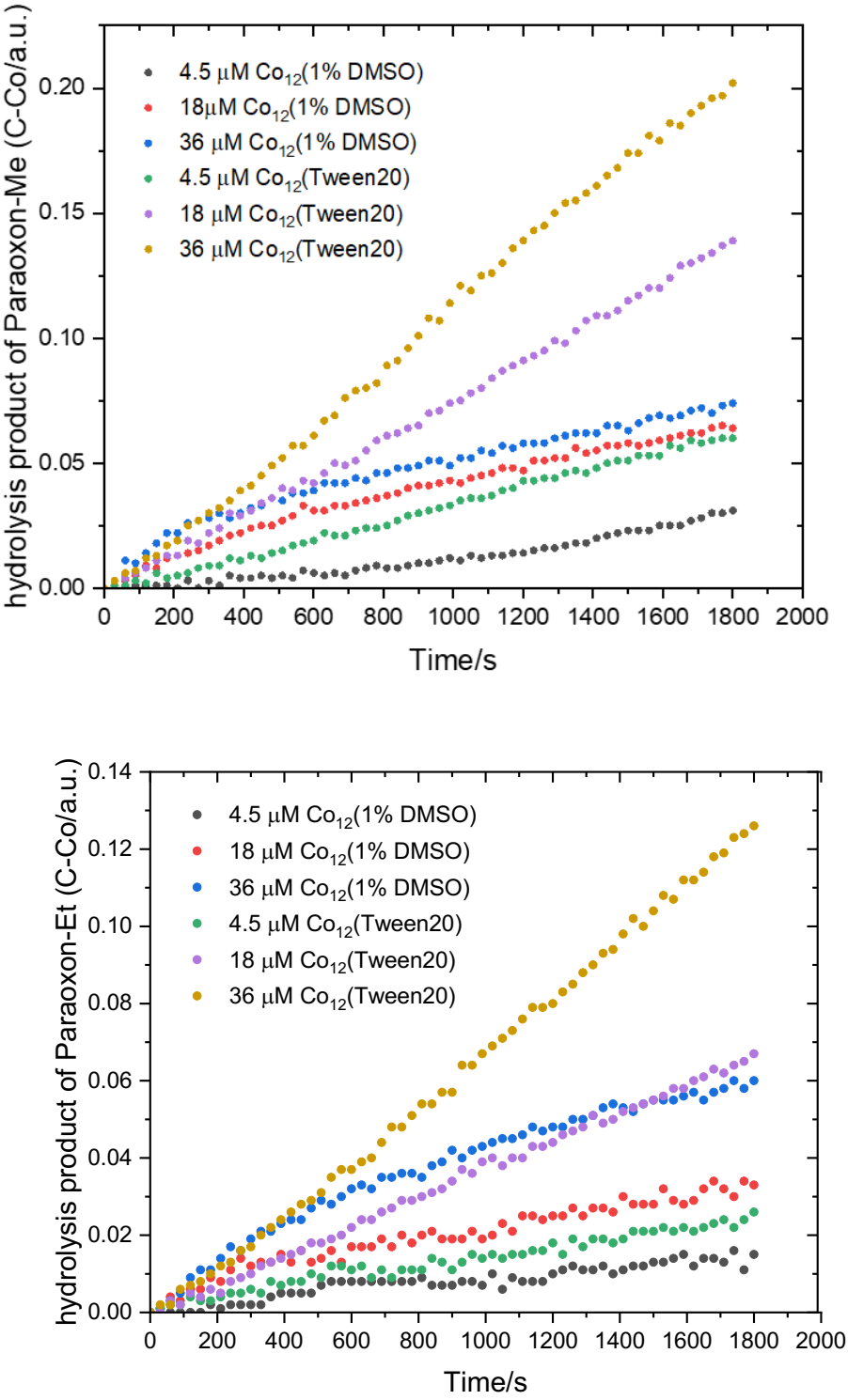

Fig. S16. Catalysed hydrolysis (pH 8, 298 K) of the phosphate esters (top) Me-paraoxon (0.45 mM) and (bottom) Et-paraoxon (0.49 mM), monitored by UV/Vis absorbance of the accumulating 4-nitrophenolate ion at 400 nm. The black, red and blue traces correspond to addition of 1, 4 and 8 mol% of **Co_{12}** (used as the **1% DMSO** water solution). The green, purple, red and yellow traces correspond to addition of 1, 4 and 8 mol% of **Co_{12}** (used as the **TW20⊂Co_{12}** solution).

4. Fluorescein degradation experiments

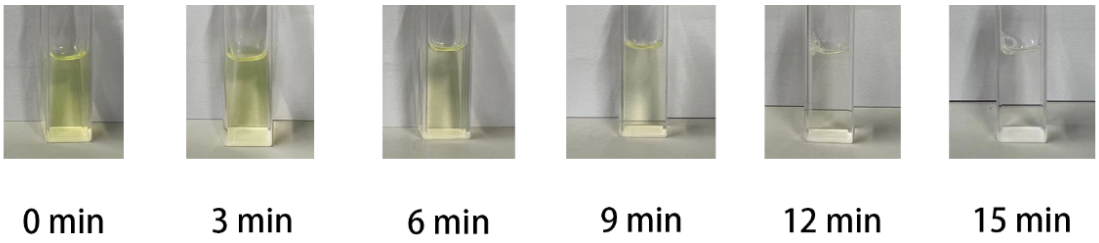

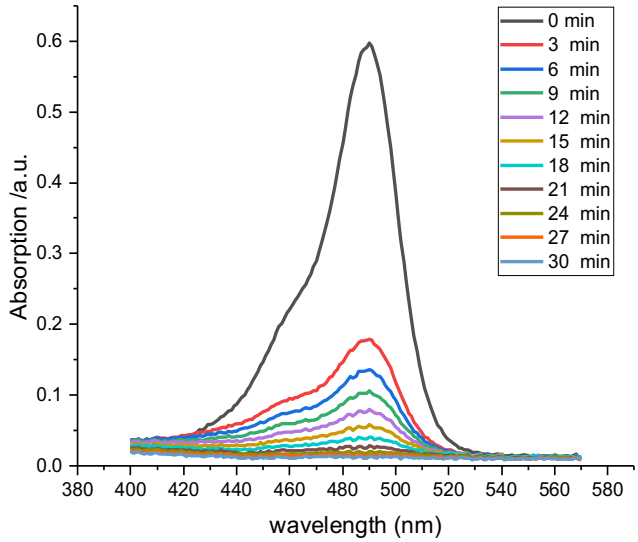

Fig. S17. Top: photos of **Co_{12}**/PMS/fluorescein solution taken at different time durations in water. Bottom: Time-dependent profiles of UV-Vis absorption spectra of fluorescein degradation. [Reaction conditions: 7.5 µM fluorescein, 337 µM PMS (45 equivalents), and 10 mol% **Co_{12}** catalyst]**.**

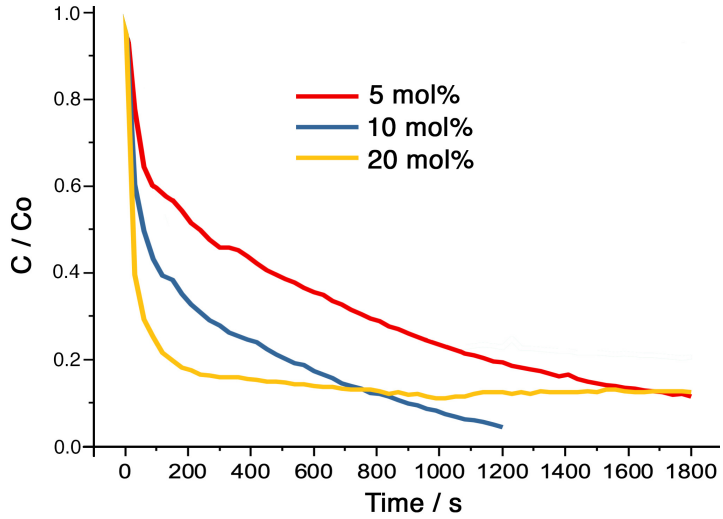

Fig. S18. Effects on reaction rates for destruction of fluorescein in water of different concentrations of **Co_{12}** catalyst [7.5 µM fluorescein, 45 equivalents of PMS (337 µM), catalyst loadings as indicated].

5. Electrochemistry

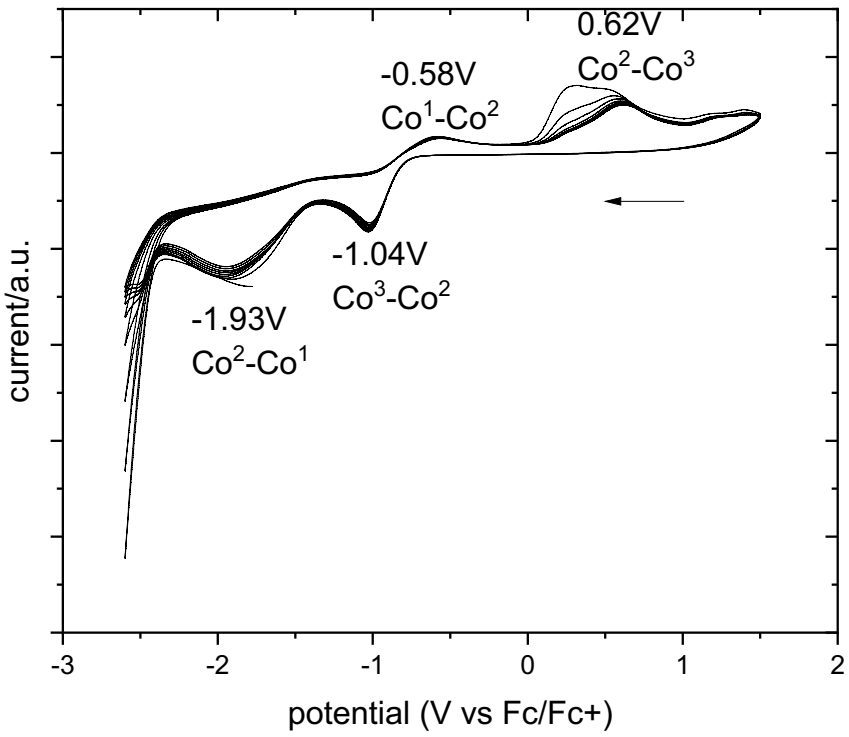

Fig. S19. Cyclic voltammogram of **Co_{12}** in MeCN at a Pt working electrode (Bu_4NPF_6 base electrolyte) showing the electrochemically irreversible Co(II)/Co(III) redox interconversion.